Available online at www.sciencedirect.com
SCIENCE DIRECT®
Journal of Molecular Graphics and Modelling 23 (2004) 89–97
Journal of Molecular Graphics and Modelling
www.elsevier.com/locate/JMGM

A molecular modeling and QSAR study of suppressors of the growth of *Trypanosoma cruzi* epimastigotes

Carlos Henrique Tomich de Paula da Silva [a,*], Sergio Marcos Sanches [b], Carlton Anthony Taft [c]

[a] *Instituto de Física de São Carlos, Universidade de São Paulo, Caixa Postal 369, São Carlos, SP, Brazil*
[b] *Instituto de Química de São Carlos, Universidade de São Paulo, São Carlos, SP, Brazil*
[c] *Centro Brasileiro de Pesquisas Físicas, Rua Dr. Xavier Sigaud, 150, CEP 22290-180, Rio de Janeiro, RJ, Brazil*

Received 4 March 2004; received in revised form 4 March 2004; accepted 5 March 2004
Available online 27 April 2004

Abstract

In this work, we have used molecular modeling and QSAR tools to study 18 dithiocarbamate suppressors of the growth of *Trypanosoma cruzi* epimastigotes, which have been reported in the literature as superoxide dismutase (SOD) inhibitors. The principal component analysis (PCA) showed that the descriptors superficial area, heat of formation, logarithm of the partition coefficient, charge of the nitrogen atom from the dithiocarbamate group and Charges of the two carbon atoms adjacent to that nitrogen are responsible for the classification between the higher and lower trypanomicid activity. Using multiple linear regression (MLR) and docking methods it was possible to identify the probable bioactive isomers that suppress of the growth of *T. cruzi* epimastigotes. Our best partial least square (PLS) model obtained with these six descriptors yields a good correlation between experimental and predicted biological activities and compares two different SODs as possible target for interaction with the dithiocarbamates.

Keywords: Superoxide dismutase; QSAR; Molecular modelling

1. Introduction

Molecular modeling and QSAR techniques have been important tools for elucidating diseases that plague humanity, such as cancer and Chaga's disease [1–3]. It is estimated that 16–18 million people are infected with the parasite *T. cruzi*, the agent of the Chaga's disease, whereas 2–3 million people have clinical symptoms that characterize the chronic stage of the disease of which 45 000 die each year [2]. Presently, treatment is not accessible to the patients during the chronic phase of the disease, which leads in 30–40% of the cases to irreversible heart and gastrointestinal lesions [3]. About one-fourth of *T. cruzi*-infected individuals develop chronic chagasic cardiomyopathy (CChC), the most severe form of the disease [4].

In regards to the Chagas' disease, many drugs have been tested which act via different mechanisms. Nifurtimox and benzonidazole were introduced in the market 25 years ago curing about 50% of the acute infections, with limited or no effects on the treatment on the chronic form of the disease, indicating collateral effects as well [5]. We emphasized, however, that a number of potential drug targets are currently under evaluation. *T. cruzi* has also been shown to be extremely sensitive, in vitro, to inhibitors of methylsteroid transferase or 24(25)-SMT, which catalyzes an essential step in the biosynthesis of steroids not present in vertebrates [6]. Enzymes of the glycolytic pathway of *T. cruzi*, present in its glycosome, have also been explored as possible targets for the drug design. One possibility is that the parasite, in the bloodstream of the host, becomes dependent on the glycolytic via for the production of energy, since the respiratory chain is relatively inefficient [5]. However, it is more likely that as the glycolytic enzymes from *T. cruzi* have extensive similarity to homologues from plant/algae [7] and are distinct from the mammalian host, they have the potential to be targeted throughout the

* Corresponding author. Tel.: +55-22-2141-7201; fax: +55-21-2141-7201.
E-mail address: catff@terra.com.br (C.H.T de Paula da Silva).

1093-3263/$ – see front matter © 2004 Elsevier Inc. All rights reserved.
doi:10.1016/j.jmgm.2004.03.013

parasites' life cycle. The trypomastigote forms of *T. cruzi* spend very little time in the bloodstream preferring to evade immune mechanisms by invading host cells. Some of these glycosomal enzymes that have been studied are the triose-phosphate isomerase (TIM) [8], glyceraldehyde-3-phosphate dehydrogenase (GAPDH) [9] and phosphoglycerate kinase (PGK) [10].

Other targets have been the Cruzipain enzyme, the major cysteine-protease present in *T. cruzi* [11], the phosphoenol-pyruvate carboxykinase, which acts on the Krebs cycle [12], and trypanothione reductase [13] as well as superoxide dismutase (SOD), the systems anti-oxidant defense [14]. Superoxide dismutases form a very conserved class of metalloenzymes that catalyzes the transformation of the cytotoxic superoxide anion, a by-product of the aerobic metabolism, in molecular oxygen and peroxide hydrogen, via alternate reduction and oxidation of the metal of the active site.

Biologically, there are three classes of superoxide dismutases, i.e., iron, manganese and copper-zinc SODs [15,16]. To date, the only valid experimental data regarding SODs indicates that only iron SODs have been biochemically characterized from any trypanosomatid. It should be noted that iron SODs are attractive drug targets as they are not found in the mammalian host.

SODs play an important role in parasitosis, acting as potent anti-oxidants that protect the parasites from the attack of the immune system of the host, which involves the production of oxidants, such as the radical superoxide [17]. Many parasites, in fact, contain this anti-oxidant, which makes attractive drug design involving the superoxide dismutase of *T. cruzi* [14,18]. Dithiocarbamates are well-known inhibitors of the superoxide dismutases containing copper and zinc at the active site [18]. In *T. cruzi*, the presence of SOD was detected, i.e., the one containing iron at the active site [14]. With the objective of determining which isomers of the dithiocarbamates investigated should inhibit the SOD present, we performed dockings studies involving these dithiocarbamates and the models of *T. cruzi* FeSOD and Cu,ZnSOD of *S. mansoni*, in addition to the chemometrical analysis.

2. Methodology

2.1. Molecular model building

The construction of the three-dimensional model for the iron superoxide dismutase (FeSOD) from *T. cruzi* followed four basic steps: (1) establishing a structure-based alignment for FeSODs/MnSODs of a known 3D structure whose coordinates were available from the Brookhaven Protein Data Bank and choice of the crystal structure on which to base the molecular framework; (2) reconstruction of the main chain and side chain coordinates for the FeSOD *T. cruzi* using the program MODELLER [19], which performs comparative protein modeling by satisfaction of spatial restraints; (3) resolution of problems of steric hindrance generated in the previous step; and (4) model evaluation.

2.1.1. Sequence alignment

As a first step in the construction of the FeSOD model from *T. cruzi*, a rigid body superposition of all FeSODs/MnSODs of a known 3D structure was performed in order to reproduce such a multiple alignment. The following SODs and their PDB codes were considered: human MnSOD (1EM1) [20]; (2) *Thermus thermophilus* MnSOD (3MDS) [21]; (3) *Mycobacterium tuberculosis* FeSOD (1IDS) [22]; (4) *Pseudomonas ovalis* FeSOD (1DT0) [23]; and (5) *Escherichia coli* FeSOD (1ISA) [24]. For the purposes of defining structurally equivalent residues in the final alignment, the histidine and aspartic acid residues of the active sites were superimposed considering their heavy atoms. In some cases, the exact alignments within the loop regions are arbitrary and do not necessarily imply conservation of conformation. The sequences for the FeSODs/MnSODs were incorporated into this alignment using the MULTALIGN program of the AMPS package [25,26], but with the restriction that all insertions and deletions were limited to regions outside the common core of α-helix and β-sheets. The crystal structure of the FeSOD from *E. coli*, solved at 1.8 Å resolution, was chosen as a template, with which the *T. cruzi* FeSOD shares 55% sequence identity.

2.1.2. Resolution of problems of steric hindrance

Problematic regions of the model were manually adjusted prior to subsequent energy minimization. This procedure was useful for relieving local bad contacts. The model had its energy minimized at various stages employing the Amber force field, within the Insight II/Discover software package [28].

The Steepest descent algorithm was used with the solvent implicitly modeled by a distance dependent dielectric constant (4r) until stereochemical and packing parameters failed to further improve. For the minimization procedure, the coordinates of the histidine and aspartic acid residues from the *T. cruzi* FeSOD active site were maintained fixed.

2.1.3. Model evaluation

During the modeling process and after the final minimization, the model was periodically evaluated for its stereochemical quality and the normality of its residue interactions and atomic contacts. The stereochemistry of the structure was evaluated using the PROCHECK program [27]. Residue environment analysis was performed with the VERIFY 3D program, which uses an implementation of the algorithms of Luthy et al. [30], and the atomic contacts were assessed with the QUALTY option of the WHATIF program [29].

2.2. Molecular descriptors

Quantum-chemical semi-empirical AM1 and PM3 calculations were performed for the lowest energy conformations of the compounds, resulting in 18 molecules.

For these dithiocarbamates reported in the literature [30], which inhibit *T. cruzi* epimastigotes, in vitro, and are shown in Fig. 3, the variables calculated by empirical and quantum-chemical semi-empirical methods were correlated with the biological activity. Isomers (conformers or optical isomers) which are the most stable for a given compound were used. Molecules such as Tc1a and Tc1b, which differ with respect to the orientations of their respective alkyl chains, present slight differences for several parameters because the moiety constituted by the dithiocarbamate group and the carbon atoms connected to the nitrogen atom is not planar. The calculated variables were total energy, highest occupied molecular orbital energy (HOMO), lowest unoccupied molecular orbital energy (LUMO), Mulliken's electronegativity, molecular hardness, molecular softness, atomic charges (from the electrostatic potential), bond orders, heat of formation, polarizability, dipole moment, ionization potential, total surface area, molecular volume, octanol–water partition coefficient ($\log P$). We also included topological [31] and three-dimensional molecular descriptors [32] with the purpose of representing different sources of chemical information in terms of size, shape of a molecule, symmetry and atom distribution in the molecule. The analysis was started with 320 molecular descriptors selected so that they represent electronic, hydrophobic, steric, topological and three-dimensional features. The geometries optimized were utilized as well as the atomic charges of the molecules, which were obtained from the electrostatic potential using MOPAC 7.0 [33]. The surface area of the molecules was calculated using the GRASP program [34]. Topological and three-dimensional descriptors were calculated using the DRAGON 4.0 program [35]. CLOGP program [36] was used to calculate the molecular lipophilicity of the corresponding carbamic acids.

2.3. Docking procedures and QSAR studies

For the docking procedures, the 18 molecules were docked with both *T. cruzi* FeSOD and *S. mansoni* Cu,ZnSOD models [37], using the DOCK 5.1 program [38]. All the chemometrical calculations were performed using the program PIROUETTE 2.02 [39].

3. Results and discussion

3.1. T. cruzi FeSOD model

Fig. 1 shows the alignment on which the structural model of *T. cruzi* FeSOD was based. The root mean square

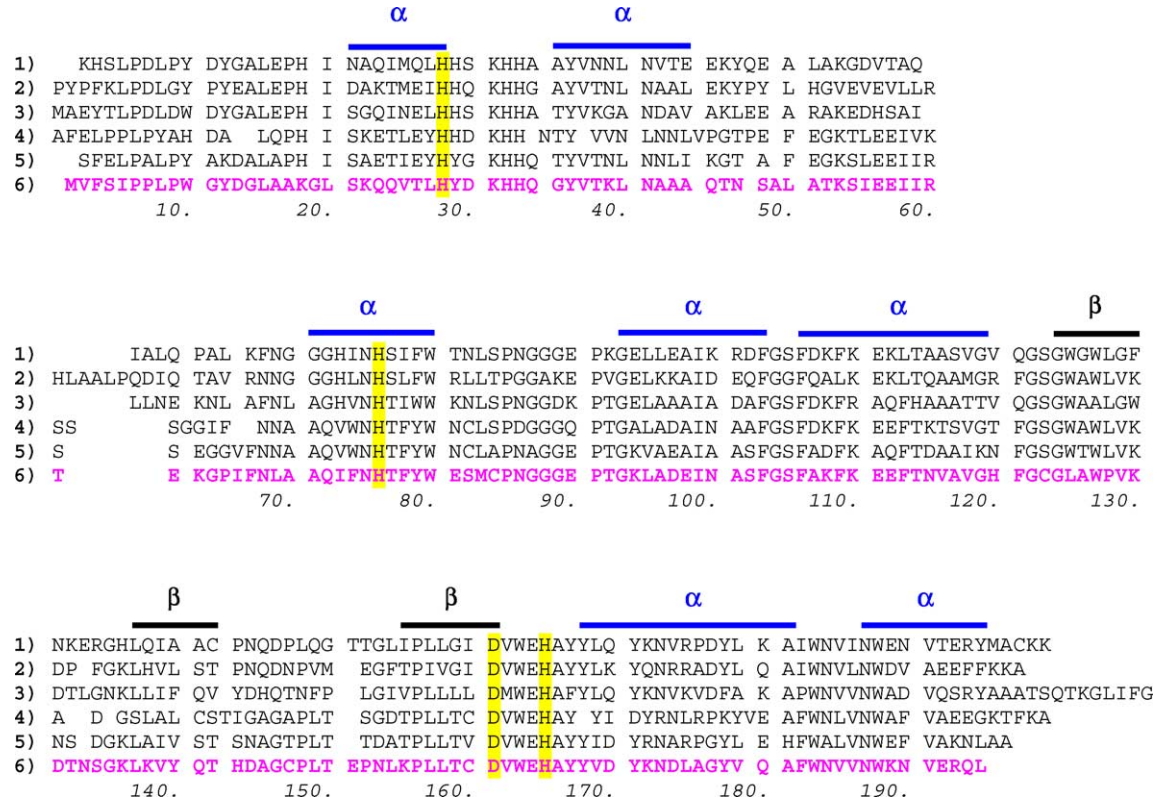

Fig. 1. Alignment of FeSOD/MnSOD sequences from PDB with the FeSOD sequence from *T. cruzi*: (1) human MnSOD (PDB code 1RFW); (2) *T. thermophilus* MnSOD (PDB code 1MSD); (3) *M. tuberculosis* FeSOD (PDB code 1IDS); (4) *P. ovalis* FeSOD (PDB code 3SDP); (5) *E. coli* FeSOD (PDB code 1ISA); and (6) *T. cruzi* FeSOD (sequence written in magenta). Above the alignment the α-helices and β-sheets are indicated with solid bars. The alignment is divided into blocks of ten residues of the sequence from *T. cruzi*. Vertical boxes (in yellow) shown on all the sequences indicate high conservations of the four active site residues which coordinate the metal.

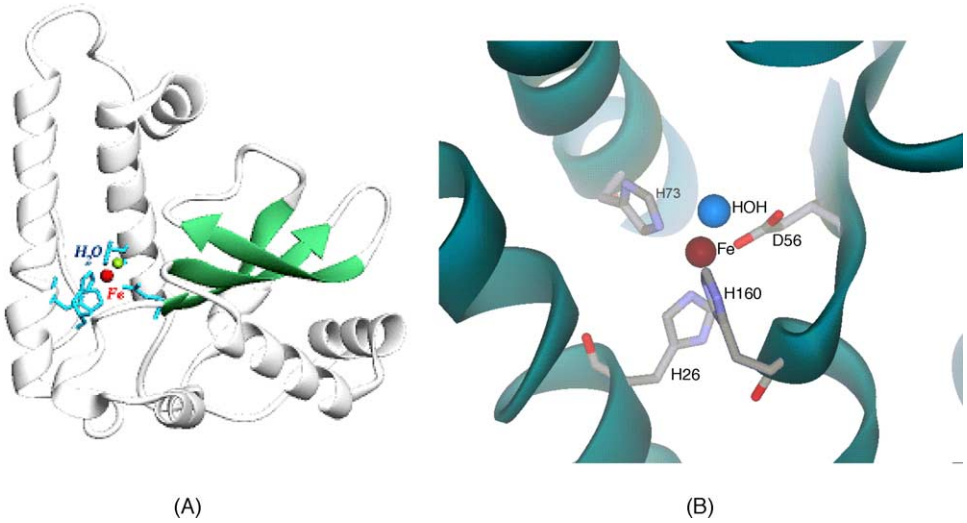

Fig. 2. (A) A ribbon diagram of the final model for the FeSOD from *T. cruzi*. The aspartic acid and the three histidines as well as the iron of the catalytic site are shown for the model structure and (B) a closeup view of the catalytic site is shown.

deviation (RMSD) for the superimposed model with each structure is 1.5 Å or lower. The final model, represented in Fig. 2, presents good stereochemistry as evaluated by the PROCHECK program [40], with a final G-factor (which evaluates the general stereochemical quality of the structure) of 0.05, above that expected for a crystal structure at 1.8 Å resolution. Model evaluation by PROCHECK indicates that 96.0% of the residues are in the most favorable regions of φ/ψ space.

Residue environment analysis (VERIFY 3D) results in a final index of 87.8, close to the average expected value of 87.9 for experimentally determined structures of proteins of such dimension, and hence well within the range for good-quality structures. Atomic contact quality as measured by

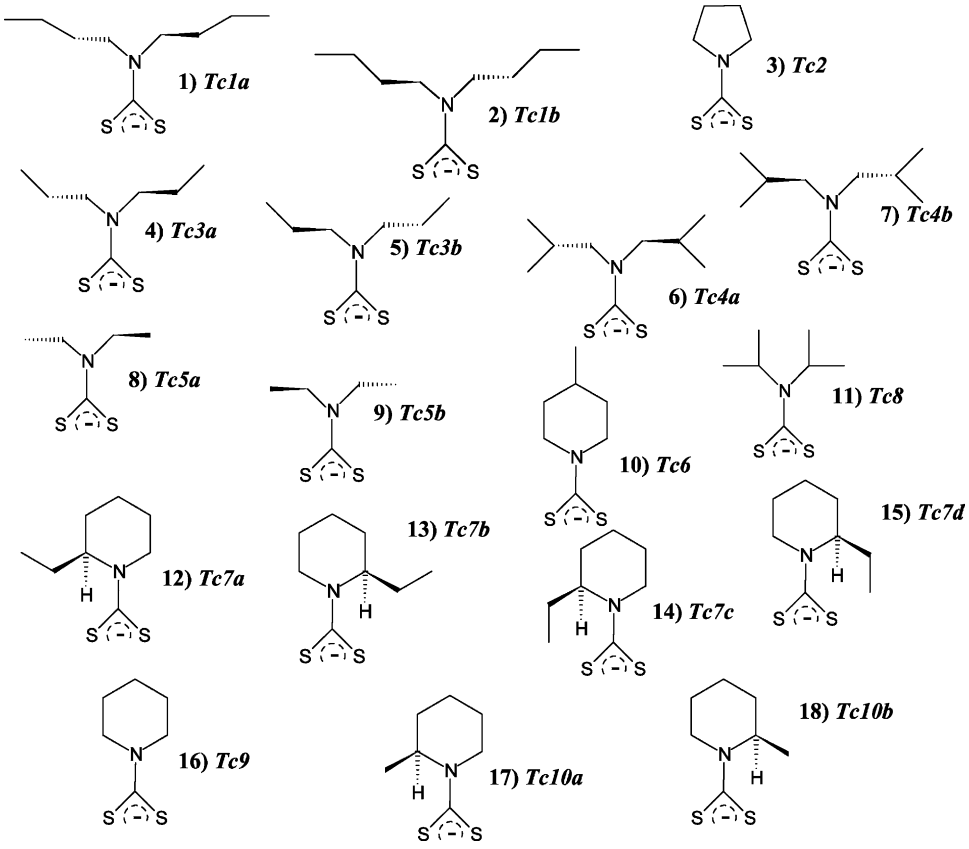

Fig. 3. *T. cruzi* epimastigotes inhibitors reported from the literature. Eighteen dithiocarbamates are cited by their codes such as Tc1–Tc18.

the QUALTY module of the WHATIF program gave a good final score of −0.78, which is well above the threshold value of −1.2, indicating good atomic contact quality.

All of the methods used for the evaluation of the model quality suggest that it presents no serious stereochemical problems or physical–chemical anomalies and that all indices are reasonable, given confidence to the final model.

3.2. QSAR studies

3.2.1. Suppressors of the growth of the T. cruzi epimastigotes

In order to give each variable equal weight in the analysis before applying the principal component analysis (PCA) and partial least square (PLS) methods, each one of the variables was autoscaled. In a first step, PCA analysis were carried out for the 18 compounds shown in Fig. 3. PCA is widely used to simplify large data sets in a way that patterns and relationships can be readily recognized and understood. The underlying purpose of the technique is the dimension reduction. After several attempts to obtain a good discrimination of the compounds in question into high activity and low activity classes, the best separation was obtained with a small set of variables. They are the total surface area (cited by SupArea), the heat of formation (HeatForm), the octanol–water partition coefficient (log P), as well as the charge of the nitrogen atom from the dithiocarbamate group (qN) and of the carbon atoms adjacent to this nitrogen (cited by qalpha1 and qalpha2). In order to distinguish the former of the second variable, qalpha1 was considered as the atomic charge of the atom closest to the sulfur atom containing the most negative charge. The adopted procedure is a mere convention in order to perform the chemometrical calculations using this observed asymmetry of charges.

For the chemometrical calculations the data set is given in Table 1. As a first step, using the chosen variables, a PLS calibration model with cross-validation was built for all the samples (the 18 molecules). Calibration curve and the plot of the studentized residual as a function of the leverage are shown in Fig. 4.

With exception of the molecule Tc2, all samples are within a 95% probability level. Using three principal components (with 93.8% of cumulated variance), the obtained linear correlation coefficient was $r = 0.857$, with a standard error of validation (SEV) = 5.15. The Tc2 molecule presented high studentized residual and high leverage, and is not so close to the calibration curve. This sample was identified as an outlier and neglected. PM3 calculation was not capable of reproducing the crystal structure of the Tc2 pyrrolidine ring [41]. Additionally, the correspondent AM1 calculation performed with Tc9 resulted in good agreement with the crystal structure of its piperydine ring. The Tc9 sample is close to the calibration curve. For similar reasons, AM1 and not PM3 calculations were selected to build the PLS model, although similar chemometrical results have been observed using both semi-empirical methods. Another PLS model was built without Tc2. The linear correlation coefficient increased to $r = 0.937$ and the SEV reduced to 3.91. As shown in Fig. 5, Tc1b is now a new outlier.

Considering that many times one of the calculated isomers contributes more than the other to the biological activity of a compound [42], successive PLS models were built, by removing, one by one, the isomers more away from the calibration curve and that presented high studentized residuals and leverages. There was improvement on the successive correlation coefficients and SEV. A final PLS model was obtained, from which it was not possible to remove any sample without reducing the quality of the resultant model. In this last model, the Tc3a and Tc3b as

Table 1
Selected variables used for the chemometrical analysis of the 18 samples[a]

Compound	Activity (%)	SupArea (Å^2)	HeatForm (kJ/mol)	log P	qN (a.u.)	qalpha1 (a.u.)	qalpha2 (a.u.)
Tc1	47.20	221.40	−42.55	3.90	0.71	−0.51	−0.58
Tc2	47.20	221.40	−42.81	3.90	1.03	−0.82	−0.99
Tc3	49.30	144.90	−15.88	1.81	0.07	−0.07	−0.03
Tc4	54.60	187.50	−31.71	3.11	0.52	−0.41	−0.37
Tc5	54.60	187.50	−32.18	3.11	0.51	−0.33	−0.39
Tc6	54.80	210.44	−41.26	3.91	0.80	−0.27	−0.30
Tc7	54.80	210.44	−41.21	3.91	0.81	−0.13	−0.17
Tc8	57.50	154.86	−21.24	2.17	0.49	−0.24	−0.23
Tc9	57.50	154.86	−21.21	2.17	0.39	−0.17	−0.23
Tc10	62.50	171.07	−26.34	2.54	0.23	−0.26	−0.26
Tc11	62.60	183.89	−30.55	3.09	0.28	−0.20	0.00
Tc12	62.60	183.89	−30.60	3.09	0.29	0.01	−0.20
Tc13	62.60	182.63	−29.78	3.09	0.43	−0.34	−0.06
Tc14	62.60	182.63	−29.78	3.09	0.41	0.04	−0.31
Tc15	63.20	175.95	−29.31	3.00	0.44	−0.12	−0.17
Tc16	66.10	155.40	−20.23	2.21	0.16	−0.22	−0.20
Tc17	66.90	169.10	−25.48	2.62	0.32	−0.22	−0.04
Tc18	66.90	169.10	−25.54	2.62	0.34	−0.06	−0.21

[a] Compounds given in Fig. 3. Activity taken from reference 30 and SupArea, HeatForm, log P, qN, qalpha1, and qalpha2 are defined in text.

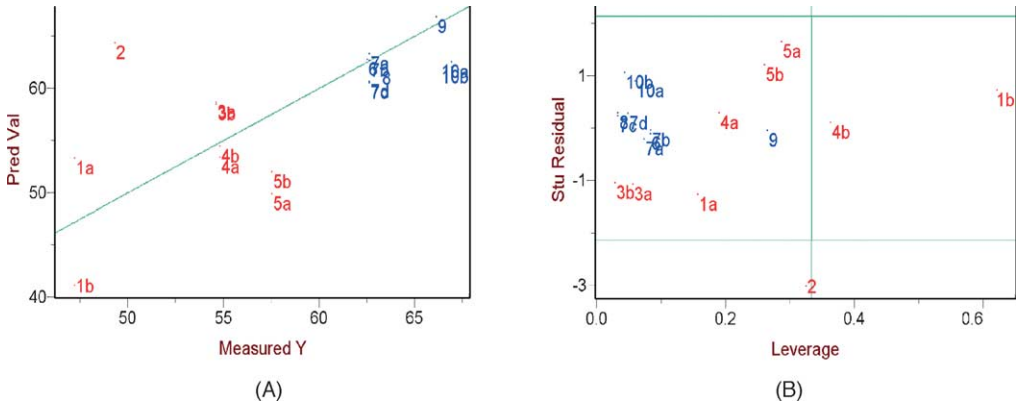

Fig. 4. (A) The PLS calibration curve and (B) the plot of the studentized residual (stu residual) as a function of the leverage. The results were obtained using all 18 molecules, for which their codes Tc were omitted. The Tc2 sample was identified as an outlier.

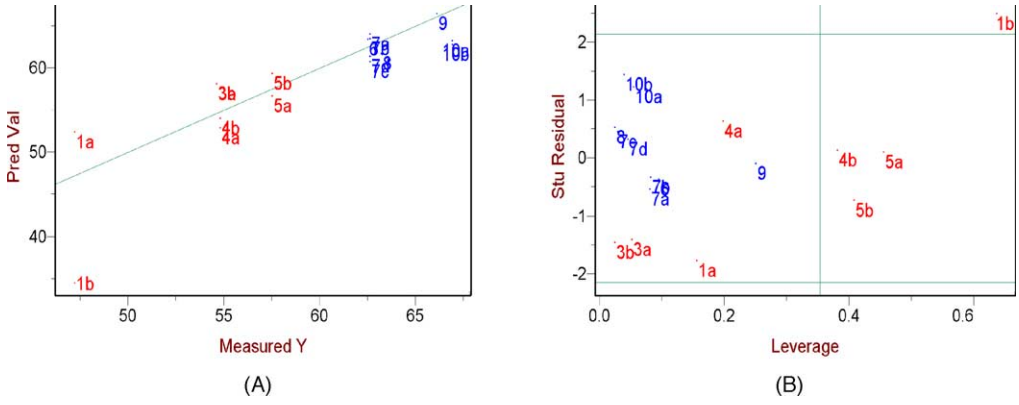

Fig. 5. (A) The PLS calibration curve, with predicted values (pred val) vs. measured values of the biological activity (measured Y), and (B) the plot of studentized residual (stu residual) as a function of the leverage. Results were obtained using all molecules (their codes Tc were omitted) with the exception of Tc2. Tc1b is now a new outlier.

well as the Tc5a and Tc5b samples indicate approximately the same distance from the calibration curve and have low studentized residuals and leverages. The resultant linear correlation coefficient was $r = 0.991$, with 95.7% of cumulated variance in the third principal component and SEV = 1.41, such as shown in Fig. 6. For the PLS models, the six selected descriptors were used here as independent variables, and the biological activity (%) as the dependent variable. Using one latent variable, the conventional Q^2 value is 0.88.

The correlation of the biological activity with the six described descriptors is shown in Eq. (1), where n represents

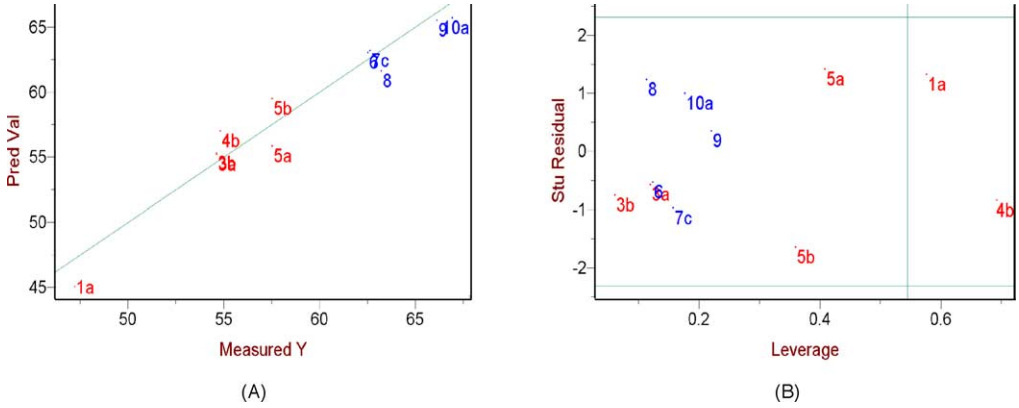

Fig. 6. (A) The final PLS calibration curve, with predicted values (pred val) vs. measured values of the biological activity (measured Y) and (B) the final plot of studentized residual (stu residual) as a function of the leverage. From this model, it was not more possible to remove any sample without reducing the quality of the resultant model.

the number of compounds, r the correlation coefficient and SEV the standard error of validation.

$$\%\,\text{Biol.Act.} = -0.113\text{SupArea} - 0.528\text{qN} + 0.107\text{qcalpha1} + 0.506\text{qcalpha2} + 0.143\text{HeatForm} + 0.353\log P \quad (1)$$

$n = 11$, $r = 0.991$, and SEV = 1.41.

Additional efforts to build new models excluding some of the isomers generated large values of SEV, without increasing the coefficient of correlation r or the information contained in the third principal component.

3.2.2. *T. cruzi* and superoxide dismutase

In *T. cruzi*, the presence of SOD was detected, i.e., the one containing iron at the active site [14]. In order to determine which SOD should be inhibited, dockings were made involving these dithiocarbamates and the *T. cruzi* FeSOD model, as well as the same compounds and the *S. mansoni* Cu,ZnSOD model. The results of the calculations are given in Table 2.

From the docking results, the contact scores obtained from DOCK 5.1 were correlated with the biological activity of the 18 molecules. Using multiple linear regression (MLR), it was possible to observe that there is practically no correlation ($r = -0.047$) of the biological activity with the contact scores of the inhibitors using the *T. cruzi* FeSOD model. The results are shown in Fig. 7. The contact scores of the same molecules using a Cu,ZnSOD model of another parasite (*S. mansoni*), yields a larger correlation with the biological activity than the previous example, with $r = 0.670$ (Fig. 8). Although the correlation values are not large enough to make definite conclusions, we note however that theoretically, even been from another parasite, the SOD containing copper and zinc at the active site seem to have more affinity for dithiocarbamates than the *T. cruzi* FeSOD model, for the same compounds.

Table 2
Contact scores (SC) of the program DOCK 5.1 for the dockings of the inhibitors of the *T. cruzi* epimastigotes, in vitro, with the *T. cruzi* FeSOD and *S. mansoni* Cu,ZnSOD (SmCT-SOD) models, and the biological activity of the 18 compounds[a]

Compound	Activity (%)	FeSODB (from *T. Cruzi*)	SmCT-SOD (from *S. mansoni*)
		SC	SC
Tc1	47.2	74.0	50.0
Tc2	47.2	58.0	50.0
Tc3	49.3	57.0	49.0
Tc4	54.6	99.0	59.0
Tc5	54.6	60.0	48.0
Tc6	54.8	101.0	61.0
Tc7	54.8	64.0	60.0
Tc8	57.5	61.0	58.0
Tc9	57.5	50.0	43.0
Tc10	62.5	69.0	52.0
Tc11	62.6	91.0	67.0
Tc12	62.6	70.0	74.0
Tc13	62.6	84.0	71.0
Tc14	62.6	77.0	77.0
Tc15	63.2	60.0	60.0
Tc16	66.1	54.0	62.0
Tc17	66.9	64.0	65.0
Tc18	66.9	58.0	73.0

[a] Compounds given in Fig. 3. Activity taken from reference [30] and FeSODB and SmCT-SOD are defined in text.

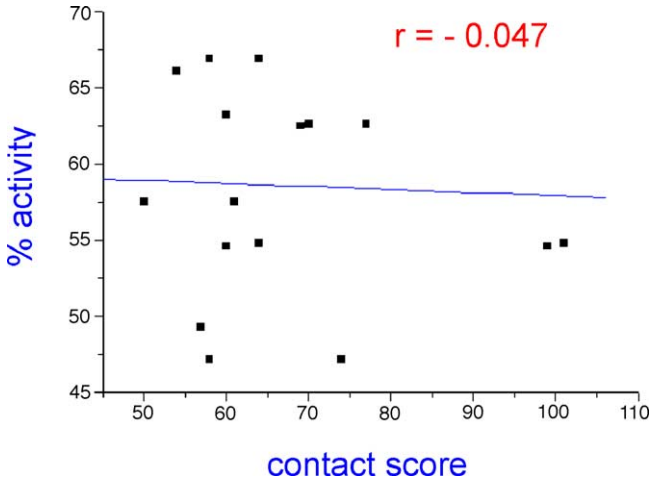

Fig. 7. Multiple linear regression between the contact scores of the suppressors of the growth of the *T. cruzi* epimastigotes, in vitro, and this biological activity (% activity). The scores were obtained from the program DOCK 5.1 for docking of the inhibitors with the *T. cruzi* FeSOD model.

The superoxide dismutases containing cofactor iron has the metal more buried than the copper in the Cu,ZnSOD structures [14–16]. The dithiocarbamates, which are compounds chelant of metals, are known inhibitors of superoxide dismutase [18]. Other potential targets for these inhibitors within the parasite were not found in the scientific literature. However, we note that dithiocarbamates are inhibitors of nuclear factor kappa B (NF-kappa B) activation

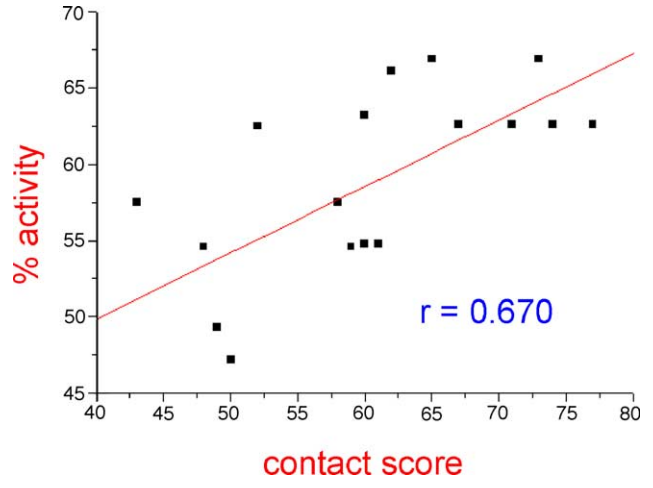

Fig. 8. Multiple linear regression between the contact scores of the suppressors of the growth of the *T. cruzi* epimastigotes, in vitro, and this biological activity (% activity). The scores were obtained from the program DOCK 5.1 for docking of the inhibitors with the *S. mansoni* Cu,ZnSOD model.

in *Ricketsia ricketsii* infection [43]. Dithiocarbamates also should bond to the SOD cofactors that contain copper at the active site more easily than iron in the FeSODs, in the event that this bond exists.

4. Conclusions

Molecular modeling and QSAR methods are important tools for analyzing the suppressors of the growth of *T. cruzi* epimastigotes as a function of the biological activity and numerous descriptors which will vary according to the inhibitors investigated. This may allow us to plan and design new and more potent inhibitors with less side effects yielding. We effectively observed from Table 1 that the larger biological activities correspond to the inhibitors 10–18, which are in general cyclic structures. We suggest that the presence of Cu,ZnSOD in *T. cruzi* be investigated. Summarizing, present QSAR results obtained in order to select the bioactive dithiocarbamates investigated in this work may have shed some additional light which could contribute to the design of more potent and selective dithiocarbamates to be used in the chemotherapeutic treatment of the Chagas' disease.

Acknowledgements

We acknowledge financial support from CNPq, FAPESP and FAPERJ. We tank Renato Murilo de Carvalho Guimarães for his participation.

References

[1] X. Fradera, X. de la Cruz, C.H.T.P. Silva, J.L. Gelpi, F.J. Luque, M. Orozco, Ligand-induced changes in the binding sites of proteins, Bioinformatics 18 (2002) 939–948.
[2] World Health Organization (who), http://www.who.int/ctd/html/chagdat.html.
[3] J.A. Urbina, G. Payares, J. Molina, C. Sanoja, A. Liendo, K. Lazardi, M.M. Piras, R. Piras, N. Perez, P. Wincker, J.F. Ryley, Cure of short- and long-term experimental Chaga's disease using D0870, Science 2731 (1996) 5277–5280.
[4] M.B.P. Soares, L.P. Carvalho, R.R. Santos, The pathogenesis of Chagas' disease: when autoimmune and parasite-specific immune responses meet, Anais da Academia Brasileira de Ciências 73 (2001) 547–559.
[5] J.C.P. Dias, J.R. Coura, in: Fiocruz (Ed.), Clínica e terapêutica da doença de Chagas, Rio de Janeiro, 1997, p. 451.
[6] R. do Campo, S.N. Moreno, S.F. Turrens, A.M. Katzin, S.M. Gonzalez-Cappa, A.O. Stoppani, Biochemical and structural alterations produced by mitoconazole and ketoconazole in *Trypanosoma cruzi*, Mol. Biochem. Parasitol. 3 (1981) 169–180.
[7] V. Hannaert, E. Saavedra, F. Duffieux, J.P. Szikora, D.J. Rigden, P.A.M. Michels, F.R. Opperdoes, Plant-like traits associated with metabolism of Trypanosoma parasites, Proc. Natl. Acad. Sci. 100 (2003) 1067–1071.
[8] R.K. Wierenga, M.E. Noble, G. Vriend, S. Nauche, W.G. Hol, Refined 1.83 Å structure of trypanosomal triosephosphate isomerase crystallized in the presence of 2.4 M ammonium sulphate. A comparison with the structure of the trypanosomal triosephosphate isomerase-glycerol-3-phosphate complex, J. Mol. Biol. 220 (1991) 995–1015.
[9] F.M.D. Vellieux, J. Hadju, C.L.M.J. Verlinde, H. Groendijk, R.J. Read, T.J. Greenhough, J.W. Campbell, Structure of glycosomal glyceraldehyde-3-phosphate dehydrogenase from *Trypanosoma-brucei* determined from Laue data, Proc. Natl. Acad. Sci. U.S.A. 90 (1993) 2355–2359.
[10] B.E. Bernstein, P.A. Michels, W.G. Hol, Synergistic effects of substrate-induced conformational changes in phosphoglycerate kinase activation, Nature 385 (1997) 275–278.
[11] M.E. Mcgrath, A.E. Eakin, J.C. Engel, J.H. Mckerrow, C.S. Craik, R.J. Fletterick, The crystal structure of cruzain: a therapeutic target for Chagas disease, J. Mol. Biol. 247 (1995) 251–259.
[12] J.J. Cazzulo, A.C. Frasch, Trans-sialidase and cruzipain: two antigens from *Trypanosoma cruzi* contain immunodominant but enzymatically inactive domains, FASEB J. 6 (1992) 3153–3161.
[13] A.H. Fairlamb, A.A. Cerami, Metabolism and functions of Trypanothione in the Kinetoplastida, Ann. Rev. Microbiol. 46 (1992) 695–729.
[14] N.J. Temperton, S.R. Wilkinson, J.M. Kelly, Cloning of an Fe-superoxide dismutase gene homologue from *Trypanosoma cruzi*, Mol. Biochem. Parasitol. 76 (1996) 339–349.
[15] M.L. Ludwig, A.L. Metzger, K.A. Pattridge, W.C. Stallings, Manganese superoxide dismutase from *Thermus thermophilus*. A structural model refined at 1. 8 Å resolution, J. Mol. Biol. 219 (1991) 335–358.
[16] L. Banci, M. Benedetto, I. Bertini, R. del Conte, M. Piccioli, M.S. Viezzoli, Solution structure of reduced monomeric Q133M2 copper, zinc superoxide dismutase (SOD). Why is SOD a dimeric enzyme? Biochemistry 37 (1998) 11780–11791.
[17] W.J. Paramchuk, S.O. Ismail, A. Bhatia, L. Gedamu, Cloning, characterization and overexpression of two iron superoxide dismutase cDNAs from *Leishmania chagasi*: role in pathogenesis, Mol. Biochem. Parasitol. 90 (1997) 203–221.
[18] N.S. Agar, J.R. Mahoney, J.W. Eaton, Hemolytic and microbicidal actions of diethyldithiocarbamic acid, Biochem. Pharmacol. 41 (1991) 985–993.
[19] A. Sali, T.L. Blundell, Comparative protein modelling by satisfaction of spatial restraints, J. Mol. Biol. 234 (1993) 779–815.
[20] U.G. Wagner, M.M. Werber, Y. Beck, J.R. Frolow, J.L. Sussman, Characterization of crystals of genetically engineered human manganese superoxide dismutase, J. Mol. Biol. 206 (1989) 787–791.
[21] M.L. Ludwig, A.L. Metzger, K.A. Pattridge, W.C. Stallings, Manganese superoxide dismutase from *Thermus thermophilus*. A structural model refined at 1.8 Å resolution, J. Mol. Biol. 219 (1991) 335–347.
[22] J.B. Cooper, H.P.C. Driessen, S.P. Wood, Y. Zhang, D. Young, Crystallization and preliminary X-ray analysis of the iron-dependent superoxide dismutase from *Mycobacterium tuberculosis*, J. Mol. Biol. 235 (1994) 1156–1166.
[23] B.L. Stoddard, P.L. Howell, D. Ringe, G.A. Petsko, The 2.1 Å resolution structure of iron superoxide dismutase *Pseudomonas ovalis*, Biochemistry 29 (1990) 8885–8901.
[24] A. Carlioz, M.L. Ludwig, W.C. Stallings, J.A. Fee, H.M. Steinman, D. Touati, Iron superoxide dismutase: nucleotide sequence of the gene from *Escherichia coli* K12 and correlation with crystal structures, J. Biol. Chem. 263 (1988) 1555–1571.
[25] G.J. Barton, M.J. Sternberg, A strategy for the rapid multiple alignment of protein sequences. Confidence levels from tertiary structure comparisons, Mol. Biol. 198 (1987) 327–337.
[26] T.A. Jones, J.Y. On, S.W. Cavan, M. Kjelgaard, Improved methods for building protein models in electron density maps and the location of errors in these models, Acta Cryst. 47A (1991) 110–119.
[27] S.J. Weiner, P.A. Kollman, D.A. Case, U.D. Singh, D. Ghio, G. Alajona, J.S. Profeta, P. Weiner, A new force field for molecular mechanical simulation of nucleic acids and proteins, J. Amer. Chem. Soc. 106 (1984) 765–784.
[28] INSIGHT II: User Guide, version 2000. Accelrys, CA.

[29] R.A. Laskowski, M.W. McArthur, J.M. Thornton, Procheck: a program to check the stereochemical quality of protein structures, J. Appl. Cryst. 26 (1993) 283–291.
[30] R. Luthy, J.U. Bowie, D. Eisenberg, Assessment of protein models with three-dimensional profiles, Nature 356 (1992) 83–85.
[31] H. van de Waterbeemd, Chemometric Methods in Molecular Design, VCH, New York, 1996.
[32] R. Todeschini, P. Gramatica, Quant. Struct.-Act. Relat. 16 (1997) 113–119.
[33] G. Vriend, Whatif: a molecular modelling and drug design program, J. Mol. Graph. 8 (1990) 52–56.
[34] R.R. Rodrigues, J.E. Lane, C.E. Carter, B.J. Bogitsh, P.K. Sjngh, L.J. Zimmerman, J.J. Molenda, M.M. Jones, Chelating agent inhibition of *Trypanosoma cruzy* epimastigotes *in vitro*, J. Inorg. Biochem. 60 (1995) 277–288.
[35] R. Todeschini, V. Consonni, A. Mauri, M. Pavan, DRAGON 4.0, Milano, Italy, 2003.
[36] J.J.P. Stewart, Mopac: a semi empirical molecular orbital program, J. Comput. -Aided Mol. Des. 4 (1990) 1–105.
[37] A. Nicholls, B. Honig, A rapid finite difference algorithm utilizing successive over-relaxation to solve the Poisson-Boltzmann equation, J. Comput. -Aided Mol. Des. 12 (1991) 345–440.
[38] A.J. Leo, Calculating log P_{oct} from structures, Chem. Rev. 93 (1993) 1281–1306.
[39] C.H.T.P. Silva, personal communication.
[40] I.D. Kuntz, Structure-based strategies for drug design and discovery, Science 257 (1992) 1078–1082.
[41] P.W.G. Newman, C.L. Raston, A.H. White, Crystallographic structure of bis(pyrrolidine-carbodithioato)–copper (II), J. Chem. Soc. Dalton Trans. 45 (1973) 1332–1338.
[42] M. Simonyi, The concept of chiral conformers and its significance in molecular pharmacology, Adv. Drug Res. 30 (1997) 73–110.
[43] D.R. Clifton, R.A. Goss, S.K. Sahni, D. van Antwerp, R.B. Baggs, V.J. Marder, D.J. Silverman, L.A. Sporn, NF-B-dependent inhibition of apoptosis is essential for host cell survival during *Rickettsia rickettsii* infection, Microbiology 95 (1998) 4646–4651.